# Simultaneous RZ-OOK to NRZ-OOK and RZ-DPSK to NRZ-DPSK format conversion in a silicon microring resonator

**Xiong, Meng; Ozolins, Oskars; Ding, Yunhong; Huang, Bo; An, Yi; Ou, Haiyan; Peucheret, Christophe; Zhang, Xinliang**

*Published in:*
Optics Express

*Publication date:*
2012

*Document Version*
Publisher's PDF, also known as Version of record

# Simultaneous RZ-OOK to NRZ-OOK and RZ-DPSK to NRZ-DPSK format conversion in a silicon microring resonator

**Meng Xiong,[1,2,*] Oskars Ozolins,[3,2] Yunhong Ding,[2] Bo Huang,[1,2] Yi An,[2] Haiyan Ou,[2] Christophe Peucheret,[2] and Xinliang Zhang[1]**

[1]*Wuhan National Laboratory for Optoelectronics, School of Optoelectronics Science and Engineering, Huazhong University of Science and Technology, Wuhan, 430074, Hubei, China*
[2]*Department of Photonics Engineering, Technical University of Denmark, 2800 Kgs. Lyngby, Denmark*
[3]*Telecommunications Institute, Riga Technical University, LV-1048 Riga, Latvia*
[*]*menxi@fotonik.dtu.dk*

**Abstract:** Simultaneous RZ-OOK to NRZ-OOK and RZ-DPSK to NRZ-DPSK modulation format conversion in a single silicon microring resonator with free spectral range equal to twice the signal bit rate is experimentally demonstrated for the first time at 41.6 Gb/s. By utilizing an optimized custom-made microring resonator with high coupling coefficient followed by an optical bandpass filter with appropriate bandwidth, good conversion performances for both modulation formats are achieved according to the converted signals eye diagrams and bit-error-rate measurements.



**OCIS codes:** (060.2330) Fiber optics communications; (060.4080) Modulation; (130.3120) Integrated optics devices; (130.7408) Wavelength filtering devices.

## References and links

1. S. Bigo, E. Desurvire, and B. Desruelle, "All-optical RZ-to-NRZ format conversion at 10 Gbit/s with nonlinear optical loop mirror," Electron. Lett. **30**(22), 1868–1869 (1994).
2. C. W. Chow, C. S. Wong, and H. K. Tsang, "All-optical RZ to NRZ data format and wavelength conversion using an injection locked laser," Opt. Commun. **223**(4–6), 309–313 (2003).
3. L. Xu, B. C. Wang, V. Baby, I. Glesk, and P. R. Prucnal, "All optical data format conversion between RZ and NRZ based on a Mach-Zehnder interferometric wavelength converter," IEEE Photon. Technol. Lett. **15**(2), 308–310 (2003).
4. L. Banchi, M. Presi, A. D'Errico, G. Contestabile, and E. Ciaramella, "All-optical 10 and 40 Gbit/s RZ-to-NRZ format and wavelength conversion using semiconductor optical amplifiers," J. Lightwave Technol. **28**(1), 32–38 (2010).
5. Y. Yu, X. L. Zhang, and D. X. Huang, "Simultaneous all-optical multi-channel RZ and CSRZ to NRZ format conversion," Opt. Commun. **284**(1), 129–135 (2011).
6. Y. Yu, B. R. Zou, W. H. Wu, and X. L. Zhang, "All-optical parallel NRZ-DPSK to RZ-DPSK format conversion at 40 Gb/s based on XPM effect in a single SOA," Opt. Express **19**(15), 14720–14725 (2011).
7. Y. Yu, X. L. Zhang, and D. X. Huang, "All-optical format conversion from CS-RZ to NRZ at 40Gbit/s," Opt. Express **15**(9), 5693–5698 (2007).
8. Y. Yu, X. L. Zhang, D. X. Huang, L. J. Li, and W. Fu, "20-Gb/s all-optical format conversions from RZ signals with different duty cycles to NRZ signals," IEEE Photon. Technol. Lett. **19**(14), 1027–1029 (2007).
9. Y. Zhang, E. M. Xu, D. X. Huang, and X. L. Zhang, "All-optical format conversion from RZ to NRZ utilizing microfiber resonator," IEEE Photon. Technol. Lett. **21**(17), 1202–1204 (2009).
10. Y. H. Ding, C. Peucheret, M. H. Pu, B. Zsigri, J. Seoane, L. Liu, J. Xu, H. Y. Ou, X. L. Zhang, and D. X. Huang, "Multi-channel WDM RZ-to-NRZ format conversion at 50 Gbit/s based on single silicon microring resonator," Opt. Express **18**(20), 21121–21130 (2010).
11. A. H. Gnauck, S. Chandrasekhar, J. Leuthold, and L. Stulz, "Demonstration of 42.7 Gb/s DPSK receiver with 45 photons/bit sensitivity," IEEE Photon. Technol. Lett. **15**(1), 99–101 (2003).
12. T. Mizuochi, K. Ishida, T. Kobayashi, J. Abe, K. Kinjo, K. Motoshima, and K. Kasahara, "A comparative study of DPSK and OOK WDM transmission over transoceanic distances and their performance degradations due to nonlinear phase noise," J. Lightwave Technol. **21**(9), 1933–1943 (2003).
13. P. Groumas, V. Katopodis, C. Kouloumentas, M. Bougioukos, and H. Avramopoulos, "All-optical RZ-to-NRZ conversion of advanced modulated signals," IEEE Photon. Technol. Lett. **24**(3), 179–181 (2012).
14. Z. Zhang, Y. Yu, and X. L. Zhang, "Simultaneous all-optical demodulation and format conversion for multi-channel (CS)RZ-DPSK signals," Opt. Express **19**(13), 12427–12433 (2011).

#174053 - $15.00 USD Received 14 Aug 2012; revised 23 Oct 2012; accepted 25 Oct 2012; published 19 Nov 2012

15. F. F. Liu, T. Wang, L. Qiang, T. Ye, Z. Y. Zhang, M. Qiu, and Y. K. Su, "Compact optical temporal differentiator based on silicon microring resonator," Opt. Express **16**(20), 15880–15886 (2008).
16. M. Xiong, Y. H. Ding, Q. Zhang, and X. L. Zhang, "All-optical clock recovery from 40 Gbit/s RZ signal based on microring resonators," Appl. Opt. **50**(28), 5390–5396 (2011).
17. X. L. Cai, D. X. Huang, and X. L. Zhang, "Numerical analysis of polarization splitter based on vertically coupled microring resonator," Opt. Express **14**(23), 11304–11311 (2006).
18. Y. H. Ding, L. Liu, C. Peucheret, J. Xu, H. Ou, K. Yvind, X. Zhang, and D. Huang, "Towards polarization diversity on the SOI platform with simple fabrication process," IEEE Photon. Technol. Lett. **23**(23), 1808–1810 (2011).

## 1. Introduction

All optical conversion between different modulation formats is required to introduce enhanced flexibility in future optical networks. Format conversion from return-to-zero (RZ) to non return-to-zero (NRZ) signals is an essential example for interfacing different parts of a future ubiquitous transparent optical network. In the past, significant efforts have been dedicated to on-off keying (OOK) RZ-to-NRZ conversion using nonlinear optical loop mirrors (NOLMs) [1], active injection locked lasers [2], or semiconductor optical amplifier (SOA) based devices [3,4] with relatively complex configurations. Single and multi-channel format conversions based on simple passive linear filter devices [5–10] have been demonstrated, however only applied to on-off keying modulation. On the other hand, because of its improved receiver sensitivity with balanced detection and superior transmission properties [11,12], differential phase shift keying (DPSK) has received special attention over the past decade. Recently, single [13] and multi-channel [14] RZ-to-NRZ format conversion for DPSK have been experimentally demonstrated using a delay interferometer (DI) with half bit delay. However the dimensions of such devices may remain prohibitively large, which would hinder their potential for integration.

Silicon photonics has received considerable attention lately due to its inherent advantages including compact size and compatibility with microelectronics fabrication processes. Silicon microring resonators (MRRs) are versatile ultra-compact devices that have been widely used for all optical signal processing [15,16].

Multiple channel RZ-OOK to NRZ-OOK format conversion based on a single silicon MRR has already been successfully demonstrated [10]. In this paper, we realize simultaneous RZ-OOK to NRZ-OOK and RZ-DPSK to NRZ-DPSK format conversion at 41.6 Gb/s based on an optimized silicon microring resonator design. We show that the use of an MRR for format conversion is compatible with DPSK modulation. We analyze the effect of the coupling coefficient of the MRR and the bandwidth of the following optical bandpass filter (OBPF) on the conversion results and then experimentally demonstrate simultaneous conversion for both OOK and DPSK formats at 41.6 Gb/s. Clear converted signals eye diagrams and bit-error-rate measurements show the good conversion performance of our scheme.

## 2. Operation principle

The principle of the format conversion is the linear filtering process at the through port of an MRR [8]. The simulated eye diagrams of RZ-OOK and RZ-DPSK signals at 41.6 Gb/s are shown in Figs. 1(a) and 1(b) respectively. The notch filtering function of the MRR is used to transform the spectrum of an RZ signal to the spectrum of an NRZ signal by suppressing specific spectral components. The spectrum of the input RZ signals (blue) and the transfer function of the MRR with FSR of 83.2 GHz at the through port (green) are shown in Fig. 1(c). When the free spectral range (FSR) of the MRR is designed to be twice the signal bit rate, RZ-OOK (respectively DPSK) can be converted to NRZ-OOK (respectively DPSK), at the expense of some amplitude ripple, as shown in Figs. 1(d)-1(f), which can be efficiently reduced by an additional optical bandpass filter (OBPF), as can be seen in Figs. 1(g)-1(i). The method has already been successfully demonstrated for RZ-OOK to NRZ-OOK conversion [10], but never so far for RZ-DPSK to NRZ-DPSK. Thanks to the frequency periodic filtering characteristic of the MRR, simultaneous conversion of both OOK and DPSK (carried on

#174053 - $15.00 USD Received 14 Aug 2012; revised 23 Oct 2012; accepted 25 Oct 2012; published 19 Nov 2012

different wavelength channels) can be realized provided the channel spacing is equal to an integer (≥2) multiple of the resonator FSR.

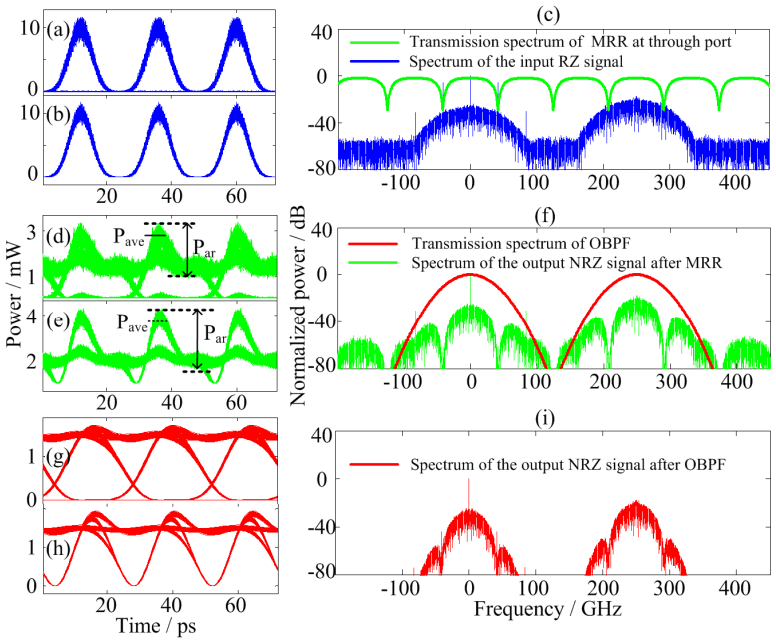


Fig. 1. Principle of the simultaneous format conversion. Eye diagrams of (a) input RZ-OOK and (b) RZ-DPSK at 41.6 Gb/s. (c) Spectrum of the input RZ signals (blue) and transfer function of the MRR with FSR of 83.2 GHz at the through port (green). Eye diagrams of (d) converted NRZ-OOK and (e) converted NRZ-DPSK after the MRR. (f) Spectrum of the converted NRZ signals after the MRR (green) and transfer function of the OBPF (red). Eye diagrams of (g) converted NRZ-OOK and (h) converted NRZ-DPSK after the OBPF. (i) Spectrum of the output NRZ signals (red) after the OBPF. In these simulations, the power coupling coefficient of the MRR is $\kappa^2 = 0.72$ and the full-width at half-maximum of the Gaussian OBPF is 60 GHz.

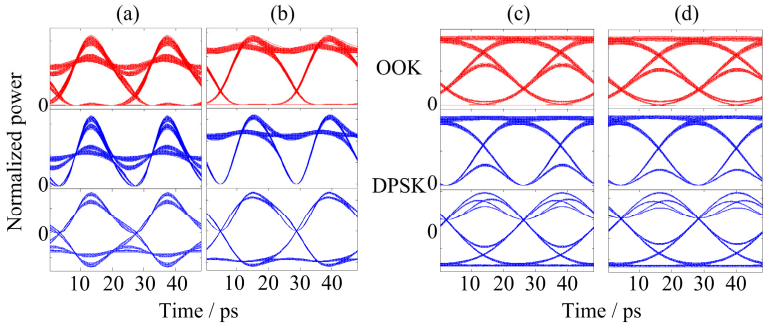


Fig. 2. Simulated eye diagrams of converted NRZ-OOK (red, top), NRZ-DPSK (blue, center), and NRZ-DPSK demodulated signals (blue, bottom) when (a) $\kappa^2 = 0.7$ and FWHM = 80 GHz, (b) $\kappa^2 = 0.9$ and FWHM = 80 GHz, (c) $\kappa^2 = 0.7$ and FWHM = 32 GHz and (d) $\kappa^2 = 0.9$ and FWHM = 32 GHz.

The amplitude ripple and the Q value of the converted NRZ signals (following interferometric demodulation and balanced detection in the case of DPSK signals) depend on the properties of the MRR and the OBPF applied for amplitude ripple mitigation. As shown in Figs. 2(a) and 2(b), when the full-width at half-maximum (FWHM) of the OBPF is 80 GHz, the amplitude ripples of the converted signal are reduced with increasing power coupling

#174053 - $15.00 USD Received 14 Aug 2012; revised 23 Oct 2012; accepted 25 Oct 2012; published 19 Nov 2012

coefficient of the MRR $\kappa^2$. Meanwhile, Figs. 2(c) and 2(d) show that the Q value of the converted signal (respectively demodulated signal) is only affected by the bandwidth of the OBPF when it is reduced to 32 GHz.

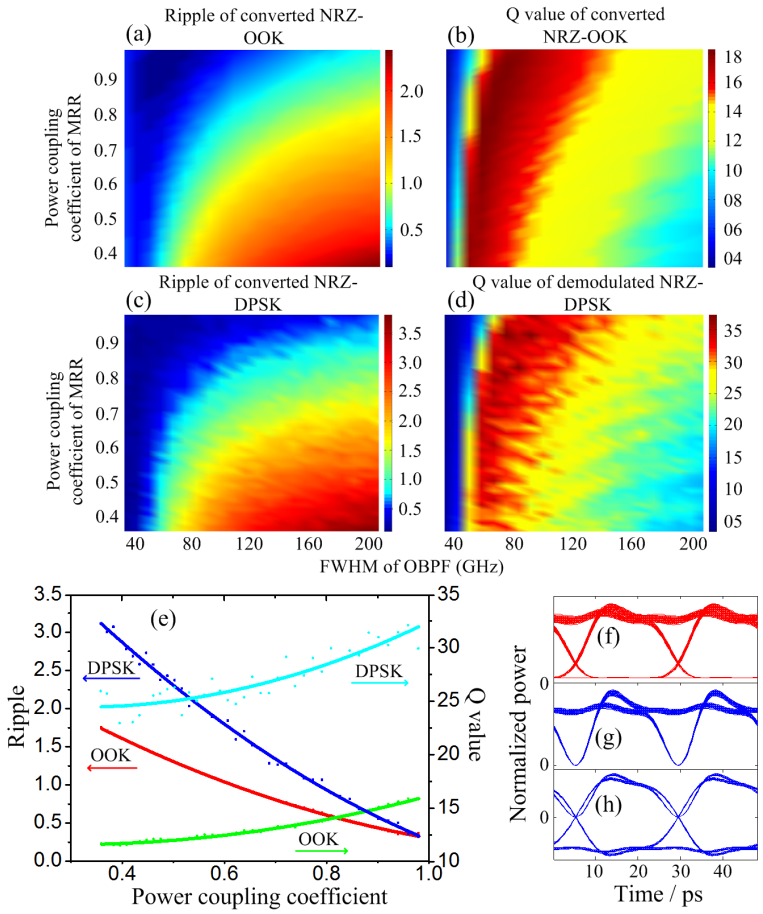


Fig. 3. (a) Calculated amplitude ripple and (b) Q value of the converted NRZ-OOK versus MRR power coupling coefficient and OBPF 3-dB bandwidth at 41.6 Gb/s. (c) Amplitude ripple of the converted NRZ-DPSK and (d) Q value of the demodulated NRZ-DPSK signal versus MRR power coupling and OBPF 3-dB bandwidth at 41.6 Gb/s. (e) Amplitude ripple and Q value versus MRR power coupling coefficient for a 1-nm OBPF. Simulated eye diagrams with optimized power coupling of 0.9 for (f) converted NRZ-OOK, (g) converted NRZ-DPSK and (h) demodulated NRZ-DPSK signal after balanced detection with an OBPF of 1 nm.

In order to generalize these observations, we have numerically evaluated the amplitude ripple and the Q value of the converted signal as a function of MRR power coupling coefficient and OBPF bandwidth, as shown in Figs. 3(a)-3(d). The amplitude ripple is defined as $P_{ar}/P_{ave}$, where $P_{ar}$ is the peak-to-peak power deviation of the high level rail in the converted eye diagram and $P_{ave}$ is its average power, as shown in Figs. 1(d) and 1(e). Fortunately, the trends of the variations of the ripple and Q value as a function of MRR power coupling coefficient and OBPF bandwidth are found to be similar for OOK and DPSK. For good conversion performance, low ripple and high Q values are required. For a fixed OBPF bandwidth of 125 GHz (~1 nm), those quantities have been simulated as a function of the MRR power coupling coefficient. As can be seen in Fig. 3(e), when the power coupling coefficient increases, the ripple decreases while the Q value becomes larger. An MRR with power coupling coefficient of 0.9 results in ripple lower than 0.8 and 0.5 and Q values higher

#174053 - $15.00 USD Received 14 Aug 2012; revised 23 Oct 2012; accepted 25 Oct 2012; published 19 Nov 2012

than 15 and 30 for the converted NRZ-OOK and DPSK signals, respectively, as shown in Figs. 3(f)-3(h).

## 3. Device design and fabrication

After having assessed the requirements on the MRR power coupling coefficient for optimum RZ-to-NRZ conversion of both OOK and DPSK formats, we focus on the design and fabrication of a suitable silicon MRR. The 3-D full vectorial film mode matching method (FMM) and coupled mode theory (CMT) [17] are used to design the MRR.

### *3.1 MRR design*

An MRR with FSR of 83.2 GHz and high power coupling coefficient is designed. As represented in Fig. 4(a), a silicon-on-insulator (SOI) wafer with a top silicon layer of 250 nm and buried silicon dioxide of 3 μm is used as the platform for MRR fabrication. The width and height of both straight and bend waveguides are 470 nm and 250 nm, respectively. Polymer (SU8-2005) is chosen for the top cladding layer. The waveguide propagation loss is assumed to be 8.2 dB/cm [10].

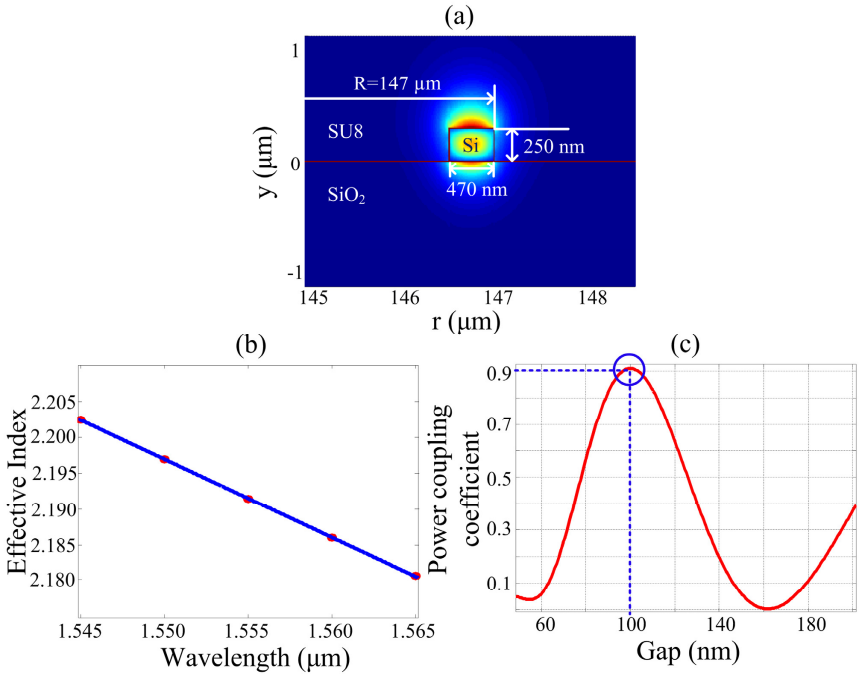


Fig. 4. (a) Cross section and transverse field distribution of the fundamental TM0 mode of the designed MRR bend rib waveguide. (b) Effective index for the TM0 mode as a function of wavelength. (c) Calculated coupling coefficient for the TM0 mode versus the width of the gap between the ring and the straight waveguide.

The structure and mode profile of the silicon waveguides are illustrated in Fig. 4(a). Figure 4(b) shows the corresponding effective index for the $TM_0$ mode as a function of wavelength. The group index is calculated to be 3.9005 at 1550 nm. The radius of the MRR is 147 μm, corresponding to an FSR of 83.2 GHz. Figure 4(c) shows the power coupling coefficient versus the dimension of the gap between the ring and the straight waveguide. We can see that a gap of around 100 nm induces a coupling coefficient higher than 0.9, as required for good conversion performance.

#174053 - $15.00 USD Received 14 Aug 2012; revised 23 Oct 2012; accepted 25 Oct 2012; published 19 Nov 2012

*3.2 MRR fabrication*

The MRR was fabricated on a SOI wafer with top silicon thickness of 250 nm and buried silica of 3 μm. Electron-beam resist ZEP520A was spin-coated on the wafer to create a 110-nm thick masking layer. The MRR structure was defined in the resist layer by electron-beam lithography. Then the patterns were transferred to the top silicon layer by inductively coupled plasma reactive ion etching (ICP-RIE). Due to the linewidth reduction of about 30 nm during the fabrication process, the waveguide width and coupling gap are designed with dimensions of 500 nm and 70 nm respectively. Figures 5(a)-5(c) show the structure of the device after fabrication. The radius of the MRR is 147 μm with waveguide width of 470 nm and coupling gap of 100 nm, as desired. To decrease the coupling loss to and from the device, a silicon nano-taper, depicted in Fig. 5(c), was adopted. A layer of 3.5 μm polymer (SU8-2005) was spin-coated on the chip. The nano-taper was defined by UV lithography and directly formed by developing. Figure 5(d) shows the measured transmission spectrum of the MRR. A low insertion loss of 8 dB is achieved with an FSR of 83 GHz and an extinction ratio (ER) of 25 dB, which corresponds to a power coupling coefficient of 0.9, as designed.

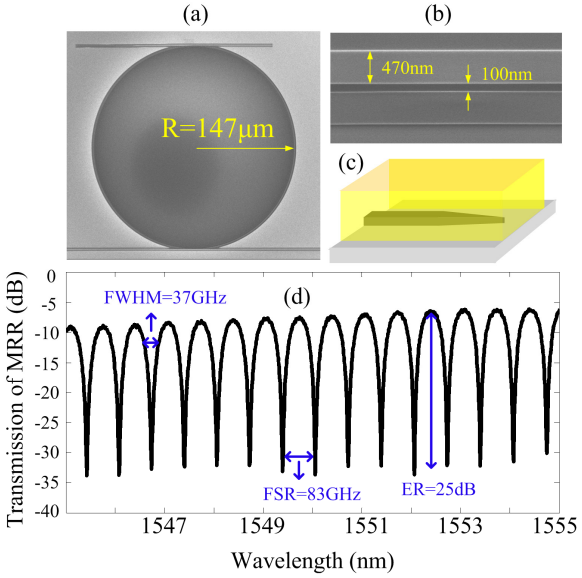


Fig. 5. Scanning electron microscope (SEM) pictures of (a) top view and (b) coupling region of the MRR. (c) Silicon nano taper design. (d) Measured transmission spectrum at the through port of the MRR.

## 4. Experimental results

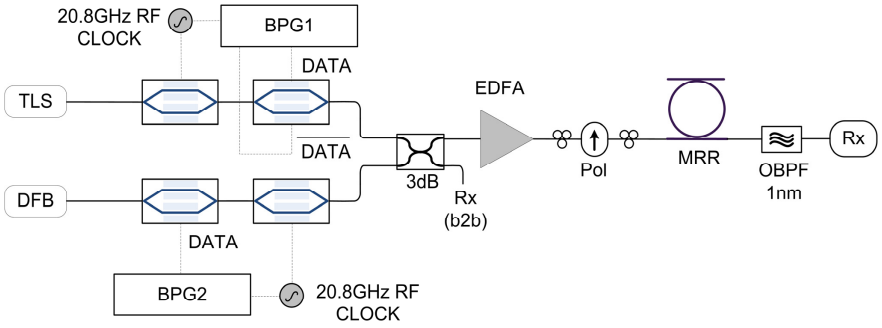


Fig. 6. Experimental setup for modulation format conversion.

#174053 - $15.00 USD Received 14 Aug 2012; revised 23 Oct 2012; accepted 25 Oct 2012; published 19 Nov 2012

The experimental setup for simultaneous RZ-to-NRZ format conversion of OOK and DPSK is shown in Fig. 6. Continuous wave light at 1549.35 nm is modulated in a Mach-Zehnder modulator (MZM) pulse carver driven by a 20.8-GHz radio frequency clock and another MZM driven with a 41.6-Gb/s pseudo-random pattern originating from a bit-pattern generator (BPG), resulting in the generation of a 33% RZ-DPSK signal at 41.6 Gb/s. Meanwhile, a 33% RZ-OOK signal centered at 1551.36 nm is generated at the same bit rate using another set of two MZMs. The pseudorandom binary sequence (PRBS) length is $2^{31}$-1 for both channels. The OOK and DPSK signals are combined in a 3-dB coupler and then amplified by an erbium-doped fiber amplifier (EDFA) to compensate the insertion loss of the modulators. Before being injected into the MRR, the states of polarization of the signals are adjusted to the TM mode of the MRR with a polarizer (Pol.) sandwiched between two polarization controllers (PCs). The converted NRZ-OOK and NRZ-DPSK signals after the MRR are filtered by an OBPF with 3-dB bandwidth of 1 nm and finally detected in a pre-amplified receiver. A 1-bit fiber DI followed by balanced detection in a pair of 45-GHz photodiodes is used for DPSK detection, while the OOK signal is detected using a single 45-GHz photodiode. The quality of the converted signals is analyzed using an optical spectrum analyzer (OSA), a 70-GHz sampling oscilloscope and an error analyzer (EA).

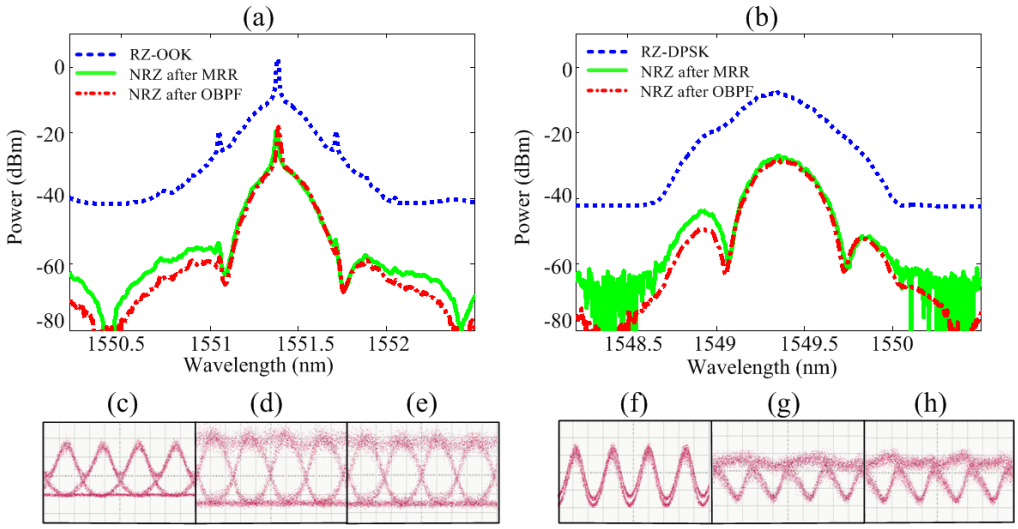


Fig. 7. Measured spectra of the single channel (a) input RZ-OOK, converted NRZ-OOK after MRR, converted NRZ-OOK after OBPF and (b) input RZ-DPSK, converted NRZ-DPSK after MRR, converted NRZ-DPSK after OBPF. The resolution bandwidth is 0.2 nm. Eye diagrams of the single channel (c) input RZ-OOK, (d) converted NRZ-OOK after MRR, (e) converted NRZ-OOK after OBPF, (f) input RZ-DPSK, (g) converted NRZ-DPSK after MRR and (h) converted NRZ-DPSK after OBPF.

Firstly the performance of the format conversion is evaluated with single channel operation by switching one of the two channels (OOK or DPSK) off. The central frequency of the input RZ signal is tuned to the center of two notches of the MRR transfer function at the through port. Figures 7(a) and 7(b) show the spectra transformation during the format conversion process for OOK and DPSK, respectively. We can see that specific spectral components of both RZ-OOK and RZ-DPSK are suppressed effectively after the MRR and their spectra are successfully transformed to the spectra of NRZ signals. However, the spectra are not significantly affected by the 1-nm OBPF. The same conclusion can be reached by observing the eye diagrams shown in Figs. 7(c)-7(e) for OOK and Figs. 7(f)-7(h) for DPSK. The amplitude ripples of the converted NRZ signals are not reduced significantly using the OBPF. This is because the bandwidth of the OBPF is relatively large while the power coupling coefficient of the MRR is sufficiently high so that the ripples of the converted NRZ signals remain small, in agreement with the numerical analysis of Figs. 3(a) and 3(c).

#174053 - $15.00 USD Received 14 Aug 2012; revised 23 Oct 2012; accepted 25 Oct 2012; published 19 Nov 2012

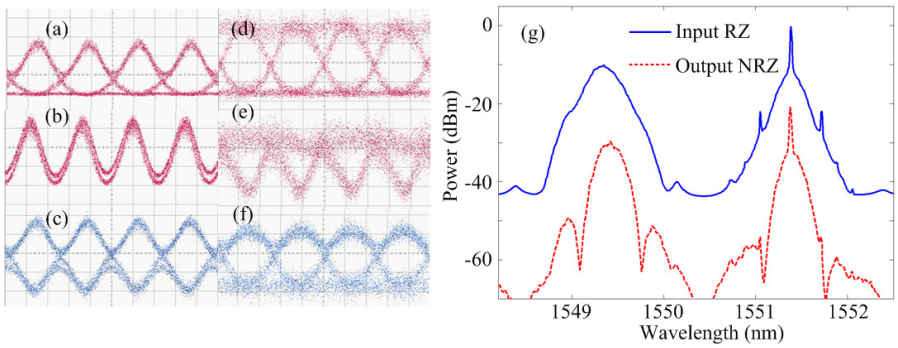


Fig. 8. Measured eye diagrams of (a) input RZ-OOK (single channel), (b) input RZ-DPSK (single channel), (c) demodulated signal of the input RZ-DPSK after balanced detection, (d) converted NRZ-OOK (two-channel), (e) converted NRZ-DPSK (two-channel) and (f) demodulated signal of the converted NRZ-DPSK after balanced detection. (g) Spectra of the two-channel input RZ signals and the converted NRZ signals (resolution bandwidth: 0.2 nm).

For the demonstration of simultaneous format conversion, the OOK and DPSK channels are both turned on. The center frequency of the OBPF is tuned to the OOK channel firstly and then to the DPSK channel prior to detection. Note that a frequency-periodic filter would be used in practice. Figures 8(a)-8(c) show the eye diagrams of the input RZ-OOK and RZ-DPSK signals and the demodulated RZ-DPSK signal after balanced detection, respectively. Figures 8(d)-8(f) show the eye diagrams of the converted NRZ-OOK, NRZ-DPSK and its demodulated signal after balanced detection, respectively. It can be seen that simultaneous format conversion is realized successfully for both channels. The corresponding spectra of the input and output signals after the MRR are shown in Fig. 8(g). The spectra of the two-channel RZ signals are transformed to those of NRZ signals simultaneously. Thanks to the high MRR power coupling coefficient, small ripples are obtained in the converted signals.

Figures 9(a) and 9(b) show the results of BER measurements for both single channel and simultaneous two-channel format conversion. It can be seen that although there is a hint of error floor, error-free performances are obtained for both OOK and DPSK channels after format conversion (the widely accepted definition of error-free corresponding to BER values below $10^{-9}$ is adopted here). In the two-channel case, the available power at the receiver was limited to −22 dBm for the converted NRZ-OOK signal, but the BER performance is strictly identical to the single channel case up to the maximum available power, corresponding to a BER of $3.5 \times 10^{-9}$. There is nearly no cross talk between the two channels. A small power penalty is measured for DPSK format conversion, while a comparatively larger power penalty of 7 dB, similar to earlier reports [10], is shown for OOK.

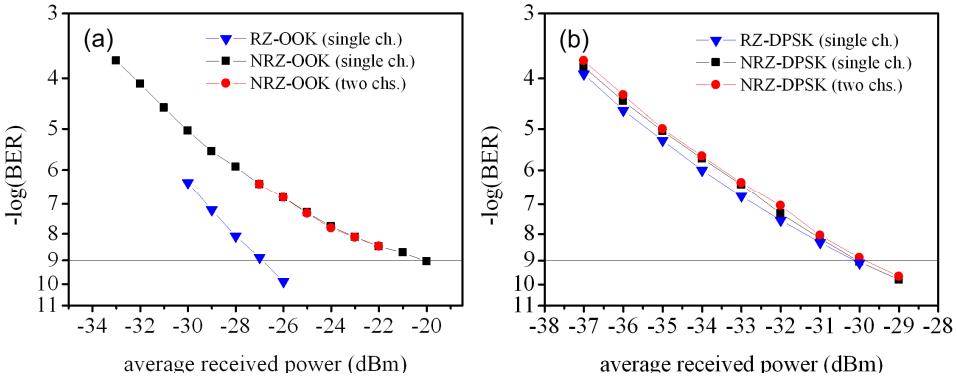


Fig. 9. BER measurements for (a) input RZ-OOK, converted NRZ-OOK for both single and two-channel operations, (b) input RZ-DPSK, converted NRZ- DPSK for both single and two-channel operations.

#174053 - $15.00 USD Received 14 Aug 2012; revised 23 Oct 2012; accepted 25 Oct 2012; published 19 Nov 2012

## 5. Discussion

Even though our experimental demonstration was performed at 41.6 Gb/s, hence with an MRR having an FSR of 83 GHz and a channel spacing of 249 GHz, the scheme is easily scalable to other channel spacings. In particular, to demonstrate the feasibility of our scheme for signal bit rates compatible with the ITU grid, we show in Fig. 10 simulation results for 100 Gb/s simultaneous conversion of RZ-OOK to NRZ-OOK and RZ-DPSK to NRZ-DPSK.

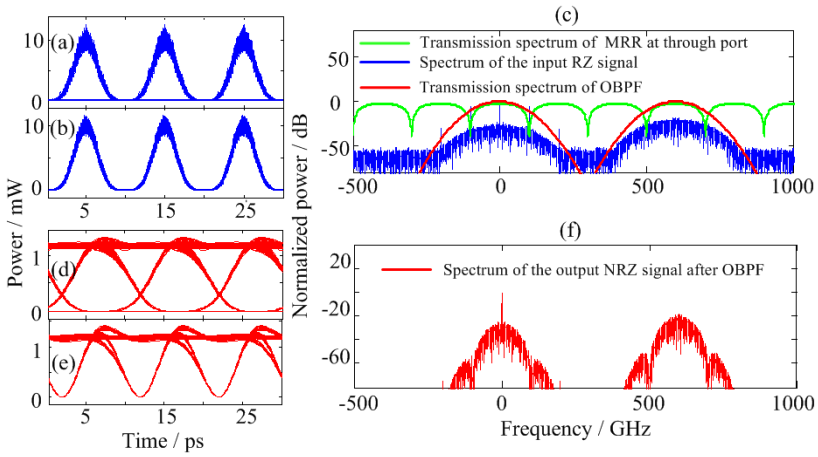


Fig. 10. 100 Gb/s simultaneous format conversion. Eye diagrams of (a) input RZ-OOK and (b) RZ-DPSK. (c) Spectrum of the input RZ signals (blue), transfer function of the MRR with FSR of 200 GHz at the through port (green) and transfer function of the OBPF (red). Eye diagrams of (d) converted NRZ-OOK and (e) converted NRZ-DPSK. (f) Spectrum of the converted NRZ signals. In the simulations, the power coupling coefficient of the MRR is $\kappa^2 = 0.9$ and the full-width at half-maximum of the Gaussian OBPF is 150 GHz.

The simulated eye diagrams of RZ-OOK and RZ-DPSK signals at 100 Gb/s are shown in Figs. 10(a) and 10(b) respectively. The spectrum of the input RZ signals (blue), transfer function of the MRR with FSR of 200 GHz at the through port (green) and the transfer function of the OBPF (red) are shown in Fig. 10(c). Simultaneous format conversion is realized successfully, as shown in Figs. 10(d)-10(f).

Compared with the MRR we used in the experiment, the cross section and the power coupling coefficient of the MRR in the simulations above remained unchanged. However, since the bit rate of the input signal is 100 Gb/s instead of 41.6 Gb/s, the radius of the MRR needs to be changed to 61 μm. Using the method introduced in Section 2, we can optimize the parameters of the MRR and the OBPF to get the best conversion performance.

Silicon chips may introduce large polarization dependences of the group index and optical coupling because of their strong confinement. The MRR we used in this paper is also polarization sensitive. However, using a polarization diversity circuit with a single microring resonator (MRR), for instance as proposed in [18], polarization independent format conversion could also be realized.

## 6. Conclusion

We have demonstrated, simultaneous RZ-to-NRZ format conversion for both OOK and DPSK signals in a well optimized custom-made silicon microring resonator with FSR of 83 GHz and power coupling coefficient of 0.9. Good converted signal quality is obtained, as attested by eye diagrams and BER measurements at 41.6 Gb/s.


## Acknowledgments

This work was sponsored by the National Natural Science Foundation of China (Grant No. 61007042), National Science Fund for Distinguished Young Scholars (No. 61125501) and the


#174053 - $15.00 USD Received 14 Aug 2012; revised 23 Oct 2012; accepted 25 Oct 2012; published 19 Nov 2012

National Basic Research Program of China (Grant No. 2011CB301704). Meng Xiong would like to thank the support of the Chinese Scholar Council (CSC). Support of the European Social Fund within the project “Support for the implementation of doctoral studies at Riga Technical University” is acknowledged.

#174053 - $15.00 USD Received 14 Aug 2012; revised 23 Oct 2012; accepted 25 Oct 2012; published 19 Nov 2012